SU(3) gauge field of magnons in antiferromagnetic skyrmion crystals

Masataka Kawano
Technical University of Munich, TUM School of Natural Sciences, Physics Department, 85748 Garching, Germany
(Dated: April 1, 2024)

Quasiparticle excitations in material solids often experience a fictitious gauge field, which can be a potential source of intriguing transport phenomena. Here, we show that low-energy excitations in insulating antiferromagnetic skyrmion crystals on the triangular lattice are effectively described by magnons with an SU(3) gauge field. The three-sublattice structure in the antiferromagnetic skyrmion crystals is inherited as three internal degrees of freedom for the magnons, which are coupled with their kinetic motion via the SU(3) gauge field that arises from the topologically nontrivial spin texture in real space. We also demonstrate that the non-commutativity of the SU(3) gauge field breaks an effective time-reversal symmetry and contributes to a magnon thermal Hall effect.

Introduction.—Quasiparticles and gauge fields are fundamental concepts for describing low-energy excitations in material solids. In certain materials, quasiparticles are not simple free particles but those with a fictitious gauge field, leading to anomalous transport phenomena. For example, electrons moving through crystals with noncoplanar spin textures experience a U(1) gauge field, namely a fictitious magnetic field, manifesting as a complex hopping [1–10]. The U(1) gauge field in real space generates a Berry curvature, fictitious magnetic field in momentum space, and contributes to the anomalous Hall effect [4–10]. Magnons, bosonic quasiparticles in magnetic insulators, can also experience a U(1) gauge field that arises from a Dzyaloshinskii-Moriya (DM) interaction or noncoplanar spin textures [11–15]. Although magnons are charge-neutral and do not feel the Lorentz force, the U(1) gauge field can bend their propagation, leading to the magnon thermal Hall effect [11–19].

The DM interactions or noncoplanar spin textures typically yield a zero net flux. In this case, the magnon systems adhere to the no-go condition that precludes the magnon thermal Hall effect in edge-shared lattice geometries such as the square and triangular lattices [12, 18]. There, due to the geometrically equivalent cells with opposite fluxes in nearest neighbors, the systems have the effective time-reversal symmetry that leaves the flux pattern unchanged while converting the sign of the thermal Hall conductivity [12, 18]. In contrast, lattices that feature corner-sharing, such as the kagome and pyrochlore lattices, escape this scenario; their geometrically inequivalent neighboring cells allow for the finite thermal Hall conductivity [12, 18].

Ferromagnetic skyrmion crystals (FM-SkXs), characterized by their topologically nontrivial swirling spin textures, yield a finite net flux, thereby contributing to the anomalous transports even in the edge-shared lattices [20–29]. The magnon thermal Hall effect is observed in the FM-SkX phase of GaV_4Se_8 [29], where $(V_4Se_4)^{5+}$ clusters form the triangular-lattice FM-SkX in the [111] plane [30–33]. Recently, the magnon thermal Hall effect is also observed in the antiferromagnetic skyrmion crystal (AFM-SkX) phase of $MnSc_2S_4$ [34], with Mn^{2+} ions forming the triangular-lattice AFM-SkX in the [111] plane [35–38]. The AFM-SkXs on the triangular lattice consist of three intertwined FM-SkXs that are antiferromagnetically coupled, leading to a three-sublattice structure [39–43]. The net flux in the AFM-SkXs, however, is naively expected to be zero because of their antiferromagnetic coupling. To explain the origin of the magnon thermal Hall effect in the AFM-SkXs, the authors in Ref. [34] introduce the concept of an SU(3) gauge field of magnons. However, how the spin textures in the AFM-SkXs are translated into the SU(3) gauge field has not yet been clarified well.

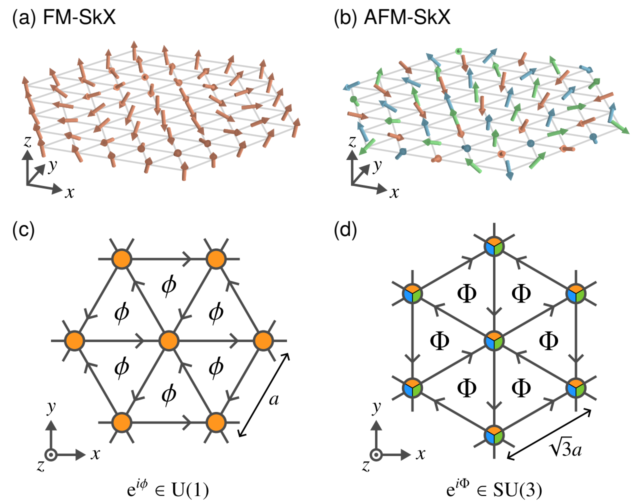

FIG. 1. **Skyrmion crystals and gauge fields of magnons.** (a), (b) Schematic illustration of the real-space spin configuration of the (a) FM-SkXs and (b) AFM-SkXs on the triangular lattice. The AFM-SkXs consist of three intertwined FM-SkXs as shown in different colors, giving rise to the three-sublattice structure. (c), (d) Schematic illustration of the uniform flux in the low-energy magnon systems for the (c) FM-SkXs and (d) AFM-SkXs. The clockwise (counterclockwise) arrows indicate the negative (positive) direction of the flux. The three different colors on each site in (d) represent the three internal degrees of freedom for the magnons. The uniform flux Φ originates from the commutation relation of an SU(3) gauge field.

In this Letter, we bridge this gap by constructing the effective field theory of magnons in the AFM-SkXs from a spin model on the triangular lattice. We show that the three sublattices in the AFM-SkXs introduce the three internal degrees of freedom for the magnons, which are coupled with their kinetic motion via the SU(3) gauge field originating from the combined effect of the spin textures of three FM-SkXs and the local antiferromagnetic coupling between them. We also find that the commutation relation of the SU(3) gauge field generates a uniformly distributed flux, which is responsible for the magnon thermal Hall effect.

Effective field theory of magnons in FM-SkXs.—Before we explore the effective field theory of magnons in the AFM-SkXs, it is instructive first to briefly discuss that in the FM-SkXs [20–29]. We start from a spin Hamiltonian on the triangular lattice,

$$\hat{\mathcal{H}} = J \sum_{\langle i,j \rangle} \hat{\boldsymbol{S}}_i \cdot \hat{\boldsymbol{S}}_j + \cdots , \tag{1}$$

where $\langle i, j\rangle$ denotes the pair of nearest-neighbor i and j sites, $\hat{\boldsymbol{S}}_i = (\hat{S}_i^x, \hat{S}_i^y, \hat{S}_i^z)$ is the spin-S operator at site i, J is the Heisenberg exchange coupling constant, and ellipsis indicates terms that stabilize the FM-SkXs (AFM-SkXs) for $J < 0$ ($J > 0$) such as a DM interaction, magnetic field, or single-ion anisotropy. We only focus on the Heisenberg exchange interaction term since the other terms do not essentially affect the following discussion.

Given the slow spatial variation of spin orientations in the FM-SkXs (see Fig. 1(a)), the low-energy theory is expected to be described by a continuously varying spin-density operator $\hat{\boldsymbol{s}}(\boldsymbol{r})$. Adopting this assumption, the effective field theory is derived by substituting $\hat{\boldsymbol{S}}_i$ with $v\hat{\boldsymbol{s}}(\boldsymbol{r})$ and $\sum_i$ with $(1/v)\int d^2\boldsymbol{r}$, where $v = \sqrt{3}a^2/2$ is the volume per site with lattice constant a. Applying these substitutions to Eq. (1) leads to the effective Hamiltonian

$$\hat{\mathcal{H}}_{\rm eff}^{\rm FM} = 3Jv \int d^2\boldsymbol{r}\, \hat{\boldsymbol{s}}(\boldsymbol{r}) \cdot \left(1 + \frac{a^2}{4}\nabla^2\right) \hat{\boldsymbol{s}}(\boldsymbol{r}), \tag{2}$$

where we drop higher-order derivative terms, which are irrelevant at low energies. To describe the magnon excitations, we employ the Holstein-Primakoff transformation [44]

$$\hat{\boldsymbol{s}}(\boldsymbol{r}) \simeq \sqrt{\frac{S}{v}} \left(\hat{b}(\boldsymbol{r})\boldsymbol{e}^-(\boldsymbol{r}) + \text{H.c.}\right) + \left(\frac{S}{v} - \hat{b}^\dagger(\boldsymbol{r})\hat{b}(\boldsymbol{r})\right)\boldsymbol{m}(\boldsymbol{r}), \tag{3}$$

where $\hat{b}(\boldsymbol{r})$ ($\hat{b}^\dagger(\boldsymbol{r})$) is the magnon annihilation (creation) operator at $\boldsymbol{r}$, $\boldsymbol{m}(\boldsymbol{r})$ is the unit vector pointing in the direction of the spin in the classical ground state, and $\boldsymbol{e}^\pm(\boldsymbol{r}) = (\boldsymbol{e}^x(\boldsymbol{r}) \pm i\boldsymbol{e}^y(\boldsymbol{r}))/\sqrt{2}$ with the unit vectors, $\boldsymbol{e}^x(\boldsymbol{r})$ and $\boldsymbol{e}^y(\boldsymbol{r})$, satisfying $\boldsymbol{e}^x(\boldsymbol{r}) \times \boldsymbol{e}^y(\boldsymbol{r}) = \boldsymbol{m}(\boldsymbol{r})$. The three unit vectors, $\boldsymbol{e}^x(\boldsymbol{r})$, $\boldsymbol{e}^y(\boldsymbol{r})$, and $\boldsymbol{m}(\boldsymbol{r})$, form a local orthonormal basis (see Fig. 2(a)). We neglect constant terms, terms quadratic in the derivative of $\boldsymbol{e}^\pm(\boldsymbol{r})$, and magnon-magnon interaction terms, which are only relevant at high energies [45, 46]. From Eqs. (2) and (3), we obtain the effective magnon Hamiltonian as

$$\hat{\mathcal{H}}_{\rm eff}^{\rm FM} \simeq \frac{3}{2}JSa^2 \int d^2\boldsymbol{r}\, \hat{b}^\dagger(\boldsymbol{r})\left(\boldsymbol{\nabla} - i\boldsymbol{A}(\boldsymbol{r})\right)^2 \hat{b}(\boldsymbol{r}), \tag{4}$$

with a U(1) gauge field $A_\mu(\boldsymbol{r}) = i\boldsymbol{e}^+(\boldsymbol{r}) \cdot \partial_\mu \boldsymbol{e}^-(\boldsymbol{r})$ ($\mu = x, y$). The associated fictitious magnetic field, $B(\boldsymbol{r}) = \partial_x A_y(\boldsymbol{r}) - \partial_y A_x(\boldsymbol{r})$, is calculated as [20–29]

$$B(\boldsymbol{r}) = \boldsymbol{m}(\boldsymbol{r}) \cdot \left(\partial_x \boldsymbol{m}(\boldsymbol{r}) \times \partial_y \boldsymbol{m}(\boldsymbol{r})\right), \tag{5}$$

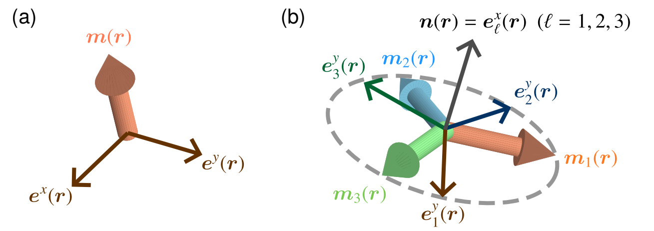

FIG. 2. **Local orthonormal basis.** (a) Local orthonormal basis in the FM-SkXs. The spatially varying $\boldsymbol{e}^x(\boldsymbol{r})$ and $\boldsymbol{e}^y(\boldsymbol{r})$ lead to the finite $\boldsymbol{A}(\boldsymbol{r})$ in the effective magnon Hamiltonian (4). (b) Three local orthonormal bases in the AFM-SkXs. The three unit vectors $\boldsymbol{m}_\ell(\boldsymbol{r})$ ($\ell = 1, 2, 3$) are on the same plane due to the local constraint $\sum_\ell \boldsymbol{m}_\ell(\boldsymbol{r}) = \boldsymbol{0}$. We take the unit vector $\boldsymbol{n}(\boldsymbol{r}) = \boldsymbol{e}^x_\ell(\boldsymbol{r})$ to be orthogonal to this plane.

which takes the finite value due to the spatial variations in $\boldsymbol{m}(\boldsymbol{r})$. Therefore, the low-energy excitations in the FM-SkXs are described by the magnons coupled with the U(1) gauge field, which arises from the spatially varying spin texture in real space [20–29].

Importantly, the topologically nontrivial spin texture in the FM-SkXs induces a uniform component of the fictitious magnetic field, $\bar{B} = (1/V)\int d^2\boldsymbol{r}\, B(\boldsymbol{r})$, which is proportional to the skyrmion density $(1/4\pi V)\int d^2\boldsymbol{r}\, \boldsymbol{m}(\boldsymbol{r}) \cdot (\partial_x \boldsymbol{m}(\boldsymbol{r}) \times \partial_y \boldsymbol{m}(\boldsymbol{r}))$, where V is the system's volume. The finite $\bar{B}$ generates magnon Landau levels and contributes to the magnon thermal Hall effect [20–29]. In terms of the original lattice, the finite $\bar{B}$ gives rise to the uniformly distributed flux $\phi = \bar{B}v/2$ as illustrated in Fig. 1(c), which breaks the effective time-reversal symmetry that prohibits the finite thermal Hall conductivity [12, 18].

We also comment on gauge redundancy. The presence of $\boldsymbol{A}(\boldsymbol{r})$ in Eq. (4) does not necessarily indicate the emergence of the U(1) gauge field, as it can also be artificially introduced by a local U(1) gauge transformation, $\hat{b}(\boldsymbol{r}) \to e^{i\varphi(\boldsymbol{r})}\hat{b}(\boldsymbol{r})$ and $\boldsymbol{A}(\boldsymbol{r}) \to \boldsymbol{A}(\boldsymbol{r}) + \boldsymbol{\nabla}\varphi(\boldsymbol{r})$. The latter transformation is equivalent to the rotation of the local orthonormal basis by $-\varphi(\boldsymbol{r})$ around $\boldsymbol{m}(\boldsymbol{r})$, leading to $\boldsymbol{e}^\pm(\boldsymbol{r}) \to e^{\pm i\varphi(\boldsymbol{r})}\boldsymbol{e}^\pm(\boldsymbol{r})$. The local U(1) gauge transformation originates from the redundancy of the description and hence all physical quantities should be gauge invariant. Therefore, the emergence of the U(1) gauge field should be characterized by finite $B(\boldsymbol{r})$, not $\boldsymbol{A}(\boldsymbol{r})$.

Effective field theory of magnons in AFM-SkXs.—We turn to the effective field theory of magnons in the AFM-SkXs. A key observation is that, since the AFM-SkXs consist of three intertwined FM-SkXs, we need to introduce three continuously varying spin-density operators $\hat{\boldsymbol{s}}_\ell(\boldsymbol{r})$ with sublattice index $\ell = 1, 2, 3$ to describe the low-energy excitations [34]. The spin operator $\hat{\boldsymbol{S}}_i$ is substituted with $v'\hat{\boldsymbol{s}}_\ell(\boldsymbol{r})$ when site i belongs to the sublattice ℓ, and $\sum_i$ is substituted with $(1/v')\int d^2\boldsymbol{r}\sum_\ell$, where $v' = 3v$. By these substitutions, we obtain the effective Hamiltonian from Eq. (1) as

$$\hat{\mathcal{H}}_{\mathrm{eff}}^{\mathrm{AFM}} = \frac{3Jv'}{2}\int d^2\boldsymbol{r}\sum_{\ell}\sum_{\ell'\neq\ell}\hat{\boldsymbol{s}}_{\ell}(\boldsymbol{r})\cdot\left(1+\frac{a^2}{4}\nabla^2\right)\hat{\boldsymbol{s}}_{\ell'}(\boldsymbol{r}). \quad (6)$$

As in the case of the FM-SkXs, we define a local orthonormal basis, $\boldsymbol{e}_{\ell}^{x}(\boldsymbol{r})$, $\boldsymbol{e}_{\ell}^{y}(\boldsymbol{r})$, and $\boldsymbol{m}_{\ell}(\boldsymbol{r})$, with sublattice index ℓ as shown in Fig. 2(b). The unit vector $\boldsymbol{m}_{\ell}(\boldsymbol{r})$ denotes the direction of the spin at $\boldsymbol{r}$ with index ℓ. To incorporate the local 120° order in the AFM-SkXs, we impose the local constraint $\sum_{\ell}\boldsymbol{m}_{\ell}(\boldsymbol{r}) = \boldsymbol{0}$, indicating that the three unit vectors $\boldsymbol{m}_{\ell}(\boldsymbol{r})$ are on the same plane. We introduce the unit vector $\boldsymbol{n}(\boldsymbol{r})$ that is orthogonal to this plane as $\boldsymbol{n}(\boldsymbol{r}) = (2/\sqrt{3})\boldsymbol{m}_1(\boldsymbol{r})\times\boldsymbol{m}_2(\boldsymbol{r})$, and take $\boldsymbol{e}_{\ell}^{x}(\boldsymbol{r}) = \boldsymbol{n}(\boldsymbol{r})$ for all $\ell = 1,2,3$, which simplifies the following calculations. Applying the Holstein-Primaloff transformation (3) with index ℓ and unit volume v' to Eq. (6) leads to the effective magnon Hamiltonian

$$\hat{\mathcal{H}}_{\mathrm{eff}}^{\mathrm{AFM}} \simeq \frac{1}{2}\int d^2\boldsymbol{r}\sum_{\ell,\ell'}\begin{pmatrix}\hat{b}_{\ell}^{\dagger}(\boldsymbol{r}) & \hat{b}_{\ell}(\boldsymbol{r})\end{pmatrix}\tilde{H}_{\ell,\ell'}(\boldsymbol{r})\begin{pmatrix}\hat{b}_{\ell'}(\boldsymbol{r})\\ \hat{b}_{\ell'}^{\dagger}(\boldsymbol{r})\end{pmatrix}, \quad (7)$$

where $\hat{b}_{\ell}(\boldsymbol{r})$ ($\hat{b}_{\ell}^{\dagger}(\boldsymbol{r})$) is the magnon annihilation (creation) operator with sublattice index ℓ and $\tilde{H}_{\ell,\ell'}(\boldsymbol{r})$ is the 2×2 matrix defined as $\tilde{H}_{\ell,\ell}(\boldsymbol{r}) = 3JS\tau^0$ for $\ell = \ell'$ and

$$\begin{aligned}\tilde{H}_{\ell,\ell'}(\boldsymbol{r}) &= \frac{3JS}{4}\left(1+\frac{a^2}{4}\nabla^2\right)(\tau^0+3\tau^x)\\ &+\frac{3JSa^2}{8}\left[\boldsymbol{A}_{\ell}(\boldsymbol{r})(\tau^y - i\tau^z) - \boldsymbol{A}_{\ell'}(\boldsymbol{r})(\tau^y + i\tau^z)\right]\cdot\boldsymbol{\nabla}\\ &+\frac{3JSa^2}{8}\left(\sum_{\ell''}\epsilon_{\ell\ell'\ell''}\right)\boldsymbol{\xi}(\boldsymbol{r})(\tau^0-\tau^x)\cdot\boldsymbol{\nabla}, \quad (8)\end{aligned}$$

for $\ell \neq \ell'$ with unit and Pauli matrices τ^{μ} ($\mu = 0, x, y, z$) and Levi-Civita symbol $\epsilon_{\ell\ell'\ell''}$. Here, we introduce four vector fields as $A_{\ell,\mu}(\boldsymbol{r}) = i\boldsymbol{e}_{\ell}^{+}(\boldsymbol{r})\cdot\partial_{\mu}\boldsymbol{e}_{\ell}^{-}(\boldsymbol{r})$ and $\xi_{\mu}(\boldsymbol{r}) = (1/3)[\boldsymbol{m}_1(\boldsymbol{r})\cdot\partial_{\mu}\boldsymbol{m}_2(\boldsymbol{r}) + \boldsymbol{m}_2(\boldsymbol{r})\cdot\partial_{\mu}\boldsymbol{m}_3(\boldsymbol{r}) + \boldsymbol{m}_3(\boldsymbol{r})\cdot\partial_{\mu}\boldsymbol{m}_1(\boldsymbol{r})]$ ($\mu = x, y$). In particular, $\boldsymbol{A}_{\ell}(\boldsymbol{r})$ can be interpreted as the U(1) gauge field arises from the FM-SkX on the sublattice ℓ.

The effective magnon Hamiltonian (7) is complicated and conceals its gauge structure. To elucidate the hidden gauge structure, we introduce new bosonic operators $\hat{\gamma}_n(\boldsymbol{r})$ ($n = 1,2,3$) as the linear combination of $\hat{b}_{\ell}(\boldsymbol{r})$ and $\hat{b}_{\ell}^{\dagger}(\boldsymbol{r})$ such that the resulting effective Hamiltonian has the following two properties; (i) the conventional 120° order, namely spatially uniform $\boldsymbol{m}_{\ell}(\boldsymbol{r})$, gives rise to three decoupled magnons with well-known linear dispersions and (ii) the equation of motion for $\hat{\gamma}_n(\boldsymbol{r})$ is relativistic, which is expected in antiferromagnets. We find the Bogoliubov transformation that satisfies these properties as

$$\hat{\gamma}_1(\boldsymbol{r}) = \frac{1}{\sqrt{3}}\sum_{\ell}\left(\cosh\chi\,\hat{b}_{\ell}(\boldsymbol{r}) + \sinh\chi\,\hat{b}_{\ell}^{\dagger}(\boldsymbol{r})\right), \quad (9)$$

$$\hat{\gamma}_2(\boldsymbol{r}) = i\sqrt{\frac{2}{3}}\sum_{\ell}\cos\theta_{\ell}\left(\cosh\chi\,\hat{b}_{\ell}(\boldsymbol{r}) + \sinh\chi\,\hat{b}_{\ell}^{\dagger}(\boldsymbol{r})\right), \quad (10)$$

$$\hat{\gamma}_3(\boldsymbol{r}) = i\sqrt{\frac{2}{3}}\sum_{\ell}\sin\theta_{\ell}\left(\cosh\chi\,\hat{b}_{\ell}(\boldsymbol{r}) + \sinh\chi\,\hat{b}_{\ell}^{\dagger}(\boldsymbol{r})\right), \quad (11)$$

with $\theta_{\ell} = 2\pi(\ell-1)/3$ and $\chi = (1/2)\mathrm{arctanh}(1/3)$. The effective Hamiltonian (7) is transformed as

$$\hat{\mathcal{H}}_{\mathrm{eff}}^{\mathrm{AFM}} \simeq \frac{1}{2}\int d^2\boldsymbol{r}\,\hat{\Psi}^{\dagger}(\boldsymbol{r})H(\boldsymbol{r})\hat{\Psi}(\boldsymbol{r}), \quad (12)$$

where $\hat{\Psi}(\boldsymbol{r}) = (\hat{\gamma}_1(\boldsymbol{r}), \hat{\gamma}_1^{\dagger}(\boldsymbol{r}), \hat{\gamma}_2(\boldsymbol{r}), \hat{\gamma}_2^{\dagger}(\boldsymbol{r}), \hat{\gamma}_3(\boldsymbol{r}), \hat{\gamma}_3^{\dagger}(\boldsymbol{r}))^T$ and

$$\begin{aligned}H(\boldsymbol{r}) = &\frac{3\sqrt{2}}{8}JSa^2\left[\tilde{I}\otimes\tau^x\nabla^2 - i\boldsymbol{T}(\boldsymbol{r})\otimes(\tau^0+3\tau^x)\cdot\boldsymbol{\nabla}\right]\\ &+\frac{9\sqrt{2}}{4}JS\,I\otimes(\tau^0+\tau^x), \quad (13)\end{aligned}$$

with $\tilde{I} = \mathrm{diag}(2,1,1)$ and $I = \mathrm{diag}(1,1,1)$. Here, we ignore terms that give higher-order contributions to the equation of motion for $\hat{\gamma}_n(\boldsymbol{r})$. The difference $\tilde{I}\neq I$ reflects the fact that one spin-wave mode has a different velocity in the 120° order phase of the triangular-lattice antiferromagnet [47]. For simplicity, we neglect this difference and replace $\tilde{I}$ with I in the following. The 3×3 matrix $T_{\mu}(\boldsymbol{r})$ ($\mu = x, y$) is given by $\boldsymbol{T}(\boldsymbol{r}) = \boldsymbol{T}^{(2)}(\boldsymbol{r})\lambda_2 + \boldsymbol{T}^{(5)}(\boldsymbol{r})\lambda_5$, where

$$\boldsymbol{T}^{(2)}(\boldsymbol{r}) = \frac{1}{3}\sum_{\ell}\boldsymbol{A}_{\ell}(\boldsymbol{r})\cos\theta_{\ell}, \quad (14)$$

$$\boldsymbol{T}^{(5)}(\boldsymbol{r}) = \frac{1}{3}\sum_{\ell}\boldsymbol{A}_{\ell}(\boldsymbol{r})\sin\theta_{\ell}, \quad (15)$$

and λ_{α} ($\alpha = 1, 2, \ldots, 8$) are Gell-Mann matrices

$$\lambda_2 = \begin{pmatrix}0 & -i & 0\\ i & 0 & 0\\ 0 & 0 & 0\end{pmatrix},\quad \lambda_5 = \begin{pmatrix}0 & 0 & -i\\ 0 & 0 & 0\\ i & 0 & 0\end{pmatrix},\quad \lambda_7 = \begin{pmatrix}0 & 0 & 0\\ 0 & 0 & -i\\ 0 & i & 0\end{pmatrix}. \quad (16)$$

Since $T_{\mu}(\boldsymbol{r})$ is Hermitian and traceless, it belongs to the Lie algebra of the SU(3) group.

The role of $\boldsymbol{T}(\boldsymbol{r})$ becomes more apparent upon deriving the equation of motion for $\hat{\gamma}(\boldsymbol{r}) = (\hat{\gamma}_1(\boldsymbol{r}), \hat{\gamma}_2(\boldsymbol{r}), \hat{\gamma}_3(\boldsymbol{r}))^T$. From the effective Hamiltonian (12), we obtain the equation of motion for $\hat{\Psi}(\boldsymbol{r},t)$ as $i\hbar\partial_t\hat{\Psi}(\boldsymbol{r},t) = (I\otimes\tau^z)H(\boldsymbol{r})\hat{\Psi}(\boldsymbol{r},t)$. Then the equation of motion for $\hat{\gamma}(\boldsymbol{r},t)$ is derived as

$$\hbar^2\frac{\partial^2}{\partial t^2}\hat{\gamma}(\boldsymbol{r},t) = \frac{27}{8}(JSa)^2\left(\boldsymbol{\nabla}I - i\boldsymbol{T}(\boldsymbol{r})\right)^2\hat{\gamma}(\boldsymbol{r},t). \quad (17)$$

For the conventional 120° order, we have $\boldsymbol{T}(\boldsymbol{r}) = \boldsymbol{0}$ and the low-energy excitations are described by three independent magnons with linear dispersion $\varepsilon(\boldsymbol{k}) \simeq (3/2)^{3/2}JSa|\boldsymbol{k}|$. For the AFM-SkXs, the real-space spin texture induces finite $\boldsymbol{T}(\boldsymbol{r})$, which couples the three species of magnons with their kinetic motion and can be interpreted as the SU(3) gauge field.

We remark that when $T_x(\boldsymbol{r})$ and $T_y(\boldsymbol{r})$ commute, there exists the unitary matrix $U(\boldsymbol{r})$ that diagonalizes $T_x(\boldsymbol{r})$ and $T_y(\boldsymbol{r})$ simultaneously, and the equation of motion (17) can be decomposed into three independent magnons with U(1) gauge fields as

$$\hbar^2\frac{\partial^2}{\partial t^2}\hat{\gamma}_n'(\boldsymbol{r},t) = \frac{27}{8}(JSa)^2\left(\boldsymbol{\nabla} - i\boldsymbol{A}_n'(\boldsymbol{r})\right)^2\hat{\gamma}_n'(\boldsymbol{r},t), \quad (18)$$

where $\hat{\gamma}'_n(\boldsymbol{r}) = \sum_{m=1}^{3} U^*_{m,n}(\boldsymbol{r})\hat{\gamma}_m(\boldsymbol{r})$ $(n = 1, 2, 3)$ and $\boldsymbol{A}'_n(\boldsymbol{r})$ is the U(1) gauge field determined by the eigenvalues of $T_\mu(\boldsymbol{r})$ $(\mu = x, y)$. Since $T_\mu(\boldsymbol{r})$ is the traceless matrix, the U(1) gauge fields satisfy $\sum_n \boldsymbol{A}'_n(\boldsymbol{r}) = \boldsymbol{0}$ and the associated magnetic fields $B'_n(\boldsymbol{r}) = \partial_x A'_{n,y}(\boldsymbol{r}) - \partial_y A'_{n,x}(\boldsymbol{r})$ cancel out each other, $\sum_n B'_n(\boldsymbol{r}) = 0$. This cancellation indicates that the net thermal Hall conductivity from three species reduces to zero. Therefore, $\boldsymbol{T}(\boldsymbol{r})$ with $[T_x(\boldsymbol{r}), T_y(\boldsymbol{r})] = 0$ does not contribute to the magnon thermal Hall effect.

Next, we consider the effect of finite $[T_x(\boldsymbol{r}), T_y(\boldsymbol{r})]$. To this end, we focus on the field strength defined as $F_{xy}(\boldsymbol{r}) = \partial_x T_y(\boldsymbol{r}) - \partial_y T_x(\boldsymbol{r}) - i[T_x(\boldsymbol{r}), T_y(\boldsymbol{r})]$, which is the counterpart of the fictitious magnetic field in the U(1) gauge field. Since $F_{xy}(\boldsymbol{r})$ belongs to the Lie algebra of the SU(3) group, it can be expanded as $F_{xy}(\boldsymbol{r}) = \sum_{\alpha=1}^{8} F^{(\alpha)}_{xy}(\boldsymbol{r})\lambda_\alpha$. The field strength is characterized by the eight real values $F^{(\alpha)}_{xy}(\boldsymbol{r})$, whose nonzero elements are calculated from Eqs. (14) and (15) as

$$F^{(2)}_{xy}(\boldsymbol{r}) = \frac{1}{3}\sum_{\ell} \cos\theta_\ell B_\ell(\boldsymbol{r}), \tag{19}$$

$$F^{(5)}_{xy}(\boldsymbol{r}) = \frac{1}{3}\sum_{\ell} \sin\theta_\ell B_\ell(\boldsymbol{r}), \tag{20}$$

$$F^{(7)}_{xy}(\boldsymbol{r}) = \frac{1}{4}\boldsymbol{n}(\boldsymbol{r}) \cdot (\partial_x \boldsymbol{n}(\boldsymbol{r}) \times \partial_y \boldsymbol{n}(\boldsymbol{r})), \tag{21}$$

where $B_\ell(\boldsymbol{r}) = \boldsymbol{m}_\ell(\boldsymbol{r}) \cdot (\partial_x \boldsymbol{m}_\ell(\boldsymbol{r}) \times \partial_y \boldsymbol{m}_\ell(\boldsymbol{r}))$ is the fictitious magnetic field on the sublattice ℓ. In particular, $F^{(7)}_{xy}(\boldsymbol{r})$ comes from the commutation relation $[T_x(\boldsymbol{r}), T_y(\boldsymbol{r})]$ and is determined by the scalar chirality of the vector field $\boldsymbol{n}(\boldsymbol{r})$.

In analogy to the case of the FM-SkXs, we focus on the uniform elements of the field strength by replacing $F^{(\alpha)}_{xy}(\boldsymbol{r})$ with $\bar{F}^{(\alpha)}_{xy} = (1/V)\int d^2\boldsymbol{r}\; F^{(\alpha)}_{xy}(\boldsymbol{r})$. $\bar{F}^{(2)}_{xy}$ and $\bar{F}^{(5)}_{xy}$ are written in terms of the average fictitious magnetic field $\bar{B}_\ell = (1/V)\int d^2\boldsymbol{r}\; B_\ell(\boldsymbol{r})$. We also assume $\bar{B}_1 = \bar{B}_2 = \bar{B}_3$ since three FM-SkXs in the AFM-SkXs typically have the same skyrmion density [39–42]. Within this approximation, $\bar{F}^{(2)}_{xy}$ and $\bar{F}^{(5)}_{xy}$ are reduced to zero, whereas $\bar{F}^{(7)}_{xy}$ takes the finite value which is proportional to the skyrmion density of the vector field $\boldsymbol{n}(\boldsymbol{r})$ defined as $(1/4\pi V)\int d^2\boldsymbol{r}\; \boldsymbol{n}(\boldsymbol{r}) \cdot (\partial_x \boldsymbol{n}(\boldsymbol{r}) \times \partial_y \boldsymbol{n}(\boldsymbol{r}))$. Returning to the original lattice, finite $\bar{F}^{(7)}_{xy}$ generates a uniformly distributed flux $\Phi = \bar{F}^{(7)}_{xy}\lambda_7 v'/2$ as shown in Fig. 1(d), which breaks the effective time-reversal symmetry and contributes to the magnon thermal Hall effect.

We finally comment on SU(3) gauge redundancy. The SU(3) gauge transformation is given by the local rotation of the internal degrees of freedom, namely $\hat{\boldsymbol{\gamma}}(\boldsymbol{r}) \to W(\boldsymbol{r})\hat{\boldsymbol{\gamma}}(\boldsymbol{r})$ and $T(\boldsymbol{r}) \to W(\boldsymbol{r})T(\boldsymbol{r})W^\dagger(\boldsymbol{r}) - i(\boldsymbol{\nabla} W(\boldsymbol{r}))W^\dagger(\boldsymbol{r})$ with $W \in$ SU(3). The latter transformation corresponds to the rotation of the vector field $F^{(\alpha)}_{xy}(\boldsymbol{r})$ in the eight-dimensional space, indicating that the length of the vector field $\sqrt{\sum_{\alpha=1}^{8}(F^{(\alpha)}_{xy}(\boldsymbol{r}))^2}$ is gauge invariant. Therefore, the emergence of the finite $F_{xy}(\boldsymbol{r})$ is not an artifact of the gauge choice and characterizes the effect of the spin texture in the AFM-SkXs.

Discussion.—We have shown that the AFM-SkXs give rise to the SU(3) gauge field of magnons, and its commutation relation leads to the uniform flux. The emergence of the uniform flux is particularly important since otherwise the no-go condition precludes a finite thermal Hall conductivity on the triangular lattice [12, 18]. Here, we briefly demonstrate this fact by considering the triangular-lattice ferromagnet with the DM interaction shown in Fig. 3(a). We assume that the direction of the spin in the classical ground state aligns with that of the DM vector $\boldsymbol{D}_{i,j}$. The DM interaction leads to the complex hopping of magnons as $J\hat{\boldsymbol{S}}_i \cdot \hat{\boldsymbol{S}}_j + \boldsymbol{D}_{i,j} \cdot (\hat{\boldsymbol{S}}_i \times \hat{\boldsymbol{S}}_j) \simeq \sqrt{J^2 + D^2}S\,(\mathrm{e}^{i\phi_{\mathrm{D}}/3}\hat{b}^\dagger_i \hat{b}_j + \mathrm{H.c.})$, where $D = |\boldsymbol{D}_{i,j}|$, $\phi_{\mathrm{D}}/3 = -\arctan(D/J)$, and $\hat{b}_i$ $(\hat{b}^\dagger_i)$ is the magnon annihilation (creation) operator at site i. The DM-induced complex hopping results in the staggered flux pattern shown in Fig. 3(b), which is preserved under a π-rotation along any straight line in the triangular lattice. This rotation, however, converts the sign of the thermal Hall conductivity, indicating that the DM-induced flux does not contribute to the magnon thermal Hall effect. The FM-SkXs and AFM-SkXs, in contrast, generate the uniform flux patterns due to the finite skyrmion density, thereby circumventing the no-go condition and contributing to the magnon thermal Hall effect.

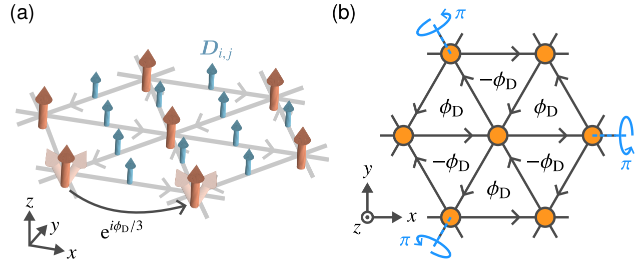

FIG. 3. **Staggered flux in the triangular-lattice ferromagnet with the DM interaction.** (a) Schematic illustration of the triangular-lattice ferromagnet with the DM interaction. Gray arrows indicate the order of spins in $\boldsymbol{D}_{i,j} \cdot (\hat{\boldsymbol{S}}_i \times \hat{\boldsymbol{S}}_j)$. The magnons acquire a phase $\phi_{\mathrm{D}}/3 = -\arctan(D/J)$ when they hop between two sites. (b) Staggered flux pattern generated by the DM interaction. The system has the π-rotation symmetry along any straight line in the triangular lattice, which prohibits the finite thermal Hall conductivity.

Conclusions and outlook.—We have shown that low-energy excitations in the AFM-SkXs on the triangular lattice are effectively governed by the magnons with the SU(3) gauge field. We have also demonstrated that the finite commutation relation of the SU(3) gauge field breaks the effective time-reversal symmetry and underpins a measurable magnon thermal Hall effect. There are several promising directions for future work. For example, it would be interesting to explore fictitious gauge fields in different classes of skyrmions [48], including two-sublattice AFM-SkXs [49–51]. Our framework is readily applicable to these systems. Elucidating how an underlying gauge structure qualitatively changes a thermal Hall conductivity would also offer an interesting research direction. Moreover, we could verify the effective field-theoretical description by comparing magnon bands and physical quantities with those obtained by the linear spin-wave theory.

Acknowledgments.—M.K. thanks C. Hotta for the discussion. M.K. was supported by JSPS Overseas Research Fellowship.

[1] X. G. Wen, F. Wilczek, and A. Zee, Chiral spin states and superconductivity, Phys. Rev. B **39**, 11413 (1989).

[2] N. Nagaosa and P. A. Lee, Normal-state properties of the uniform resonating-valence-bond state, Phys. Rev. Lett. **64**, 2450 (1990).

[3] P. A. Lee and N. Nagaosa, Gauge theory of the normal state of high-T_c superconductors, Phys. Rev. B **46**, 5621 (1992).

[4] P. Matl, N. P. Ong, Y. F. Yan, Y. Q. Li, D. Studebaker, T. Baum, and G. Doubinina, Hall effect of the colossal magnetoresistance manganite $La_{1-x}Ca_xMnO_3$, Phys. Rev. B **57**, 10248 (1998).

[5] J. Ye, Y. B. Kim, A. J. Millis, B. I. Shraiman, P. Majumdar, and Z. Tešanović, Berry Phase Theory of the Anomalous Hall Effect: Application to Colossal Magnetoresistance Manganites, Phys. Rev. Lett. **83**, 3737 (1999).

[6] K. Ohgushi, S. Murakami, and N. Nagaosa, Spin anisotropy and quantum Hall effect in the kagomé lattice: Chiral spin state based on a ferromagnet, Phys. Rev. B **62**, R6065 (2000).

[7] S. H. Chun, M. B. Salamon, Y. Lyanda-Geller, P. M. Goldbart, and P. D. Han, Magnetotransport in Manganites and the Role of Quantal Phases: Theory and Experiment, Phys. Rev. Lett. **84**, 757 (2000).

[8] Y. Lyanda-Geller, S. H. Chun, M. B. Salamon, P. M. Goldbart, P. D. Han, Y. Tomioka, A. Asamitsu, and Y. Tokura, Charge transport in manganites: Hopping conduction, the anomalous Hall effect, and universal scaling, Phys. Rev. B **63**, 184426 (2001).

[9] Y. Taguchi and Y. Tokura, Enhancement of anomalous Hall effect in a filling-changed pyrochlore-type molybdate, Europhys. Lett. **54**, 401 (2001).

[10] Y. Taguchi, Y. Oohara, H. Yoshizawa, N. Nagaosa, and Y. Tokura, Spin Chirality, Berry Phase, and Anomalous Hall Effect in a Frustrated Ferromagnet, Science **291**, 2573 (2001).

[11] S. Fujimoto, Hall Effect of Spin Waves in Frustrated Magnets, Phys. Rev. Lett. **103**, 047203 (2009).

[12] H. Katsura, N. Nagaosa, and P. A. Lee, Theory of the Thermal Hall Effect in Quantum Magnets, Phys. Rev. Lett. **104**, 066403 (2010).

[13] Y. Onose, T. Ideue, H. Katsura, Y. Shiomi, N. Nagaosa, and Y. Tokura, Observation of the Magnon Hall Effect, Science **329**, 297 (2010).

[14] S. A. Owerre, Topological thermal Hall effect in frustrated kagome antiferromagnets, Phys. Rev. B **95**, 014422 (2017).

[15] P. Laurell and G. A. Fiete, Topological Magnon Bands and Unconventional Superconductivity in Pyrochlore Iridate Thin Films, Phys. Rev. Lett. **118**, 177201 (2017).

[16] R. Matsumoto and S. Murakami, Theoretical Prediction of a Rotating Magnon Wave Packet in Ferromagnets, Phys. Rev. Lett. **106**, 197202 (2011).

[17] R. Matsumoto and S. Murakami, Rotational motion of magnons and the thermal Hall effect, Phys. Rev. B **84**, 184406 (2011).

[18] T. Ideue, Y. Onose, H. Katsura, Y. Shiomi, S. Ishiwata, N. Nagaosa, and Y. Tokura, Effect of lattice geometry on magnon Hall effect in ferromagnetic insulators, Phys. Rev. B **85**, 134411 (2012).

[19] M. Hirschberger, R. Chisnell, Y. S. Lee, and N. P. Ong, Thermal Hall Effect of Spin Excitations in a Kagome Magnet, Phys. Rev. Lett. **115**, 106603 (2015).

[20] K. A. van Hoogdalem, Y. Tserkovnyak, and D. Loss, Magnetic texture-induced thermal Hall effects, Phys. Rev. B **87**, 024402 (2013).

[21] L. Kong and J. Zang, Dynamics of an Insulating Skyrmion under a Temperature Gradient, Phys. Rev. Lett. **111**, 067203 (2013).

[22] J. Iwasaki, A. J. Beekman, and N. Nagaosa, Theory of magnon-skyrmion scattering in chiral magnets, Phys. Rev. B **89**, 064412 (2014).

[23] Y.-T. Oh, H. Lee, J.-H. Park, and J. H. Han, Dynamics of magnon fluid in Dzyaloshinskii-Moriya magnet and its manifestation in magnon-Skyrmion scattering, Phys. Rev. B **91**, 104435 (2015).

[24] A. Roldán-Molina, A. S. Nunez, and J. Fernández-Rossier, Topological spin waves in the atomic-scale magnetic skyrmion crystal, New J. Phys. **18**, 045015 (2016).

[25] A. Mook, B. Göbel, J. Henk, and I. Mertig, Magnon transport in noncollinear spin textures: Anisotropies and topological magnon Hall effects, Phys. Rev. B **95**, 020401 (2017).

[26] S. K. Kim, K. Nakata, D. Loss, and Y. Tserkovnyak, Tunable Magnonic Thermal Hall Effect in Skyrmion Crystal Phases of Ferrimagnets, Phys. Rev. Lett. **122**, 057204 (2019).

[27] P. Nikolić, Quantum field theory of topological spin dynamics, Phys. Rev. B **102**, 075131 (2020).

[28] T. Weber, D. M. Fobes, J. Waizner, P. Steffens, G. S. Tucker, M. Böhm, L. Beddrich, C. Franz, H. Gabold, R. Bewley, D. Voneshen, M. Skoulatos, R. Georgii, G. Ehlers, A. Bauer, C. Pfleiderer, P. Böni, M. Janoschek, and M. Garst, Topological magnon band structure of emergent landau levels in a skyrmion lattice, Science **375**, 1025 (2022).

[29] M. Akazawa, H.-Y. Lee, H. Takeda, Y. Fujima, Y. Tokunaga, T.-h. Arima, J. H. Han, and M. Yamashita, Topological thermal Hall effect of magnons in magnetic skyrmion lattice, Phys. Rev. Res. **4**, 043085 (2022).

[30] I. Kézsmárki, S. Bordács, P. Milde, E. Neuber, L. Eng, J. White, H. Rønnow, C. Dewhurst, M. Mochizuki, K. Yanai, H. Nakamura, D. Ehlers, V. Tsurkan, and A. Loidl, Néel-type skyrmion lattice with confined orientation in the polar magnetic semiconductor GaV4S8, Nat. Mater. **14**, 1116 (2015).

[31] E. Ruff, S. Widmann, P. Lunkenheimer, V. Tsurkan, S. Bordács, I. Kézsmárki, and A. Loidl, Multiferroicity and skyrmions carrying electric polarization in GaV¡sub¿4¡/sub¿S¡sub¿8¡/sub¿, Sci. Adv. **1**, e1500916 (2015).

[32] Y. Fujima, N. Abe, Y. Tokunaga, and T. Arima, Thermodynamically stable skyrmion lattice at low temperatures in a bulk crystal of lacunar spinel GaV_4Se_8, Phys. Rev. B **95**, 180410 (2017).

[33] S. Bordács, A. Butykai, B. G. Szigeti, J. S. White, R. Cubitt, A. O. Leonov, S. Widmann, D. Ehlers, H.-A. K. von Nidda, V. Tsurkan, A. Loidl, and I. Kézsmárki, Equilibrium Skyrmion Lattice Ground State in a Polar Easy-plane Magnet, Sci. Rep. **7**, 7584 (2017).

[34] H. Takeda, M. Kawano, K. Tamura, M. Akazawa, J. Yan, T. Waki, H. Nakamura, K. Sato, Y. Narumi, M. Hagiwara, M. Yamashita, and C. Hotta, Magnon thermal Hall effect via emergent SU(3) flux on the antiferromagnetic skyrmion lattice, Nat. Commun. **15**, 566 (2024).

[35] S. Reil, H.-J. Stork, and H. Haeuseler, Structural investigations of the compounds ASc2S4 (A=Mn, Fe, Cd), J. Alloy. Compd. **334**, 92 (2002).

[36] V. Fritsch, J. Hemberger, N. Büttgen, E.-W. Scheidt, H.-A. Krug von Nidda, A. Loidl, and V. Tsurkan, Spin and Orbital Frustration in $MnSc_2S_4$ and $FeSc_2S_4$, Phys. Rev. Lett. **92**, 116401 (2004).

[37] S. Gao, O. Zaharko, V. Tsurkan, Y. Su, J. White, G. Tucker, B. Roessli, F. Bourdarot, R. Sibille, D. Chernyshov, T. Fennell, A. Loidl, D.C., and C. Rüegg, Spiral spin-liquid and the emergence of a vortex-like state in $MnSc_2S_4$, Nature Phys. **13**, 157 (2017).

[38] S. Gao, H. D. Rosales, F. A. G. Albarracin, G. K. Tsurkan, T. Fennell, P. Steffens, M. Boehm, P. Cermak, A. Schneldewind, E. Ressouche, D. Cabra, C. Rüegg, and O. Zaharko, Fractional antiferromagnetic skyrmion lattice induced by anisotropic couplings, Nature **586**, 37 (2020).

[39] H. D. Rosales, D. C. Cabra, and P. Pujol, Three-sublattice skyrmion crystal in the antiferromagnetic triangular lattice, Phys. Rev. B **92**, 214439 (2015).

[40] S. A. Díaz, J. Klinovaja, and D. Loss, Topological Magnons and Edge States in Antiferromagnetic Skyrmion Crystals, Phys. Rev. Lett. **122**, 187203 (2019).

[41] A. Mukherjee, D. S. Kathyat, and S. Kumar, Antiferromagnetic skyrmion crystals in the Rashba Hund's insulator on triangular lattice, Sci. Rep. **11**, 9566 (2021).

[42] M. Mohylna, F. A. Gómez Albarracín, M. Žukovič, and H. D. Rosales, Spontaneous antiferromagnetic skyrmion/antiskyrmion lattice and spiral spin-liquid states in the frustrated triangular lattice, Phys. Rev. B **106**, 224406 (2022).

[43] S. Hayami, Three-sublattice antiferro-type and ferri-type skyrmion crystals in centrosymmetric magnets, arXiv:2310.10834 (2023).

[44] T. Holstein and H. Primakoff, Field Dependence of the Intrinsic Domain Magnetization of a Ferromagnet, Phys. Rev. **58**, 1098 (1940).

[45] M. E. Zhitomirsky and A. L. Chernyshev, Colloquium: Spontaneous magnon decays, Rev. Mod. Phys. **85**, 219 (2013).

[46] A. Mook, J. Klinovaja, and D. Loss, Quantum damping of skyrmion crystal eigenmodes due to spontaneous quasiparticle decay, Phys. Rev. Res. **2**, 033491 (2020).

[47] T. Jolicoeur and J. C. Le Guillou, Spin-wave results for the triangular Heisenberg antiferromagnet, Phys. Rev. B **40**, 2727 (1989).

[48] B. Göbel, I. Mertig, and O. A. Tretiakov, Beyond skyrmions: Review and perspectives of alternative magnetic quasiparticles, Phys. Rep. **895**, 1 (2021).

[49] X. Zhang, Y. Zhou, and M. Ezawa, Antiferromagnetic Skyrmion: Stability, Creation and Manipulation, Sci. Rep. **6**, 24795 (2016).

[50] B. Göbel, A. Mook, J. Henk, and I. Mertig, Antiferromagnetic skyrmion crystals: Generation, topological Hall, and topological spin Hall effect, Phys. Rev. B **96**, 060406 (2017).

[51] S. Hayami, Antiferro Skyrmion Crystal Phases in a Synthetic Bilayer Antiferromagnet under an In-Plane Magnetic Field, J. Phys. Soc. Jpn. **92**, 084702 (2023).